

# EXPERIMENTAL CHARACTERIZATION OF A FLEXIBLE MEMBRANE FLAPPING-WING IN FORWARD FLIGHT

**Wang Liguang, Song Bifeng, Yang Wenqing, Fu Peng**  
**School of aeronautics, Northwestern Polytechnical University, Xi'an, China, 710072**

## Abstract

*This paper presents a multidisciplinary experimental study to characterize a flexible flapping-wing by investigating the relationship between deformation and production of aerodynamic forces through series of wind tunnel experiments. The experimental setup consists of a flapping mechanism for single-degree-of-freedom flapping actuation and with input/output power and flapping kinematics measurement, a high responsive load cell for measuring the lift and thrust, and a unique digital image correlation system that consists of only one camera and a stereo vision spectroscope for capturing the structural deformation. Technical challenges of setting up experimental system for driving and measuring are resolved in this study, aerodynamic loads, wing kinematics, and wing deformations are synchronously measured. Intensive data analyses are performed to extract useful information from the experimental results, strong correlations between passive deformation and aerodynamic performance are revealed.*

## 1 Introduction

The flapping-wing micro air vehicles (FMAV) have the revolutionary operation capabilities necessary for the future micro air vehicles (MAV) [1]. The high maneuverability with the ability to hover as well as forward flight, and the aerodynamic advantages of flapping flight [2],[3], are the most attractive features for the surveillance operations in restrictive urban environment. The Northwestern Polytechnical University (NWPU) has developed a series of

electric-motor-powered vehicles using membrane flapping-wings sizing from 30 to 60 cm. The latest one is already able to operate automatically and transmit live colored video, with an endurance of 15 minutes at a cruise speed of 10 m/s.

The characteristics of the flexible membrane flapping-wing are strongly affected by the flapping-wing's unsteady dynamics and the aeroelastic properties. The aerodynamics is determined by a wing's geometry and the kinematics. On the other hand, the kinematics and the induced inertia forces, combined with aerodynamic forces, alter a flexible wing's geometry. This interactive problem is so complex, computational challenges remain to be solved. In order to have a better understanding of flapping-wing, experimental investigation seems to be a reasonable alternative to characterize it.

A significant amount of FMAV research has focused on interaction between structure, aerodynamic, and inertial forces. Measuring a flexible flapping-wing's dynamic deformation used to be a dominant problem until the imaging correlation technologies been developed.

Zeng and Wang et al. developed a method using patterns of laser lines projected onto a flying object to reconstruct the wing's kinematic parameters [4],[5]. Walker et al. used direct linear transformation (DLT) methods to investigate the kinematics of flapping-wing in tethered locusts and freely flying hoverflies [6],[7]. These studies measured the twist and camber deformations of flapping wings, and aerodynamic consequences of the twist and camber deformations were analyzed in Ref. [8] using computational fluid dynamics simulations with the Fluent™ software.

Wu et al. developed a digital image correlation (DIC) method for tracking the motion of membrane flapping wings. Aerodynamic forces were also measured by a force-and-torque load cell; Results show that the thrust and parameters of the wing-tip deformation phase loops are strongly correlated.

The work of this paper carries out a multidisciplinary study of the kinematics and aerodynamics of a membrane flapping-wing. Flexible deformations, dynamic forces, and flapping kinematics are synchronously measured in a series of wind tunnel experiments. The effects of flapping frequency and free stream velocity on time variations of kinematic parameters, deformations, and aerodynamic forces in flapping wings are investigated.

## 2 Experimental Setup

### 2.1 Flapping Mechanism and Test Model

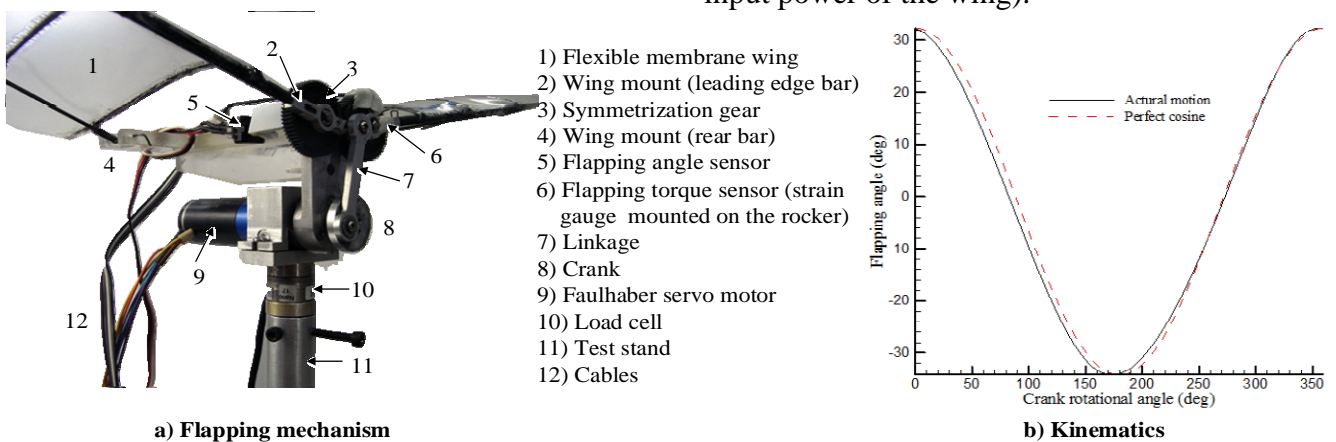


Fig. 1 Flapping mechanism

The test wing is shown in Fig. 2. The planform of the wing is combined by a rectangle and an ellipse, with an aspect ratio of 4.5, a 200 mm wing length and a 100 mm root chord. The wing is with camber of the upper profile of airfoil E378, in order to mimic the geometric features of bird wing. The wing is constructed with unidirectional carbon fiber to form the skeleton and tear-resistant polyether film as the membrane. The leading edge spar and the diagonal batten are off-the-shelf carbon rods with diameter of 2 mm and 1.8 mm,

This study developed a single-DOF flapping mechanism as shown in Fig. 1. The mechanism is driven by a Faulhaber motor system that includes a brushless servo motor 2036, a 43:1 reduction ratio planetary gearbox, a 1024 counts hall-effect encoder and a CAN controller. The motor system actively regulates the motor by using the close-loop control algorithm, and provides precise control of rotational speed and rotational angle. The output speed of the motor with the gear box ranges from 0 to 17 revolutions per second. The rotation from the motor is transformed into a reciprocating flapping motion by a simple four-bar-linkage mechanism with a flapping amplitude  $\Phi$  of 66.6 degree. The right side rocker is driven by the linkage directly, and the left side rocker is driven by a pair of symmetrization gear. The actual flapping angle can be measured by a rotational potentiometer which is coaxially mounted to the rocker. An additional torque sensor is mounted on the rocker to measure the output power of the flapping mechanism (or the input power of the wing).

respectively. The rib of the wing is formed in a die with unidirectional carbon fiber. The cross section shape of the rib is semi-circle. Ribs are distributed proportionally along the spanwise with the gap of 40 mm, and are placed parallel with the free stream. The parts of the skeleton are tied together with thread and glued with resin. A biaxially oriented polyether film called Orkesta™ is applied to the finished skeleton by using polyurethane adhesive. The high elastic modulus (1.08–1.37GPa) and tear-resistant properties make it possible to make no support

for the trailing edge. The root of the wing for mount are reinforced with a steel bar in leading edge and steel wire in diagonal batten. The total weight of a single wing is 5.7g.

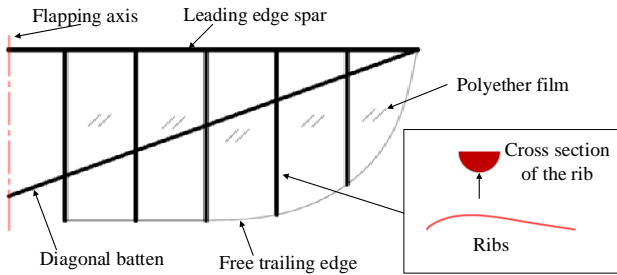


Fig. 2 Geometry of the test wing

## 2.2 Wind Tunnel Setup

Experiments are conducted in a 1.05 m×1.2 m in-draft open circuit extremely low turbulence wind tunnel located at the Northwestern Polytechnical University (NWPU). The inlet has a contraction ratio of 22.6:1, and test section length is 2.8 m, as shown in Fig. 3. Tunnel turbulence level at the mid test section is 0.02% when the speed is 3~35m/s.



Fig. 3 Wind tunnel and test model mount

A six-component load cell is used to measure the aerodynamic forces produced by the wings. Compared with normal wind tunnel balances, the load cell is able to measure at high response and have a high resolution for small forces. An industrial sensor Nano17 SI-12-0.12 from ATI Automation, Inc. is selected to replace the balance the wind tunnel used (as Fig. 1 shown). The measurement range is 12 N and a resolution of 1/320 N in both the thrust ( $F_x$ ) and the lift ( $F_z$ ) directions, which is adequate for the current experiments.

The angle of attack (AOA) of the experiments is set to 5 degrees, and the wind speed ranges from 0 to 8 m/s, as well as the flapping frequency ranges from 4 to 8 Hz.

## 2.3 Digital Image Correlation System

It seems that there are no better options than noncontact vision-based technologies to capture the wing structural deformations, since the wing is lightweight and, thus, any sensor mount on the surface of the membrane will change its deflection properties. In this work, DIC technology is used to capture the wing structural deformation.

Similar studies have been done by Wu and Cheng et al. [9], [10], [11], they used DIC technology to capture the deformation of the flapping-wing and applied more than one camera to build up stereo vision. But we found that there are some disadvantages of using multi-video stream cameras in our previous attempts. First, it is hard to guarantee that all cameras would work synchronously, even they are declared internally synchronized. Buffer overflow and transmission lag may be the reason of asynchronously, especially when high resolution and high speed are simultaneously required. Second, the combination of aperture and the shutter speed of the camera is crucial for capturing a sharp enough picture, it is also hard to keep the picture both sharp and bright enough. For example, in this study, the flapping amplitude of the wing tip is up to 220 mm, so the aperture should be kept as small as possible to obtain the sufficient depth of field. On the other hand, the flapping frequency is up to 8 Hz (in this case, the speed of wing tip is up to 6.2 m/s), the shutter speed of the camera should be no less than 1/2000 to ‘freeze’ the motion. This combination of aperture and shutter speed must be an underexposure setting, even we used four 470 Lux cold light illuminator to lighten the object. Third, the system composition is slightly complex by using multi-cameras. A large number of cables, additional data acquisition cards, and higher performance computers are required. The feasibility to mount excessive devices as cameras, tripods, and powerful light sources around or inside the wind tunnel, is also not easy to be settled.

For these reasons, a new method by using a single camera for capturing stereo-images is developed in this study. A Canon™ camera for photograph is applied instead of pairs of video

stream cameras. An adjustable single-lens dual optical path spectroscopy is produced to obtain stereo-images, as shown in Fig. 4.

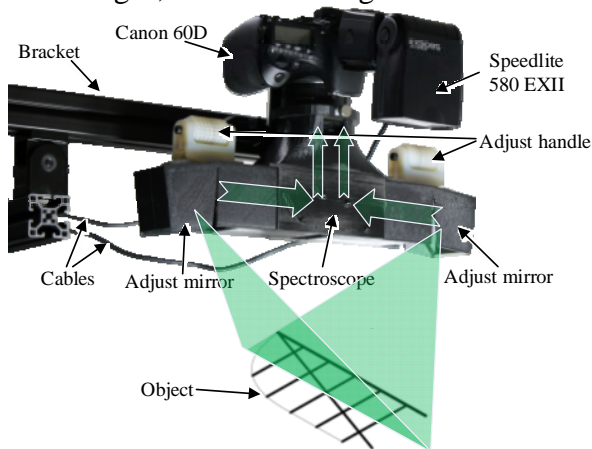


Fig. 4 DIC system setup

The mirrors used in this system are aluminum film reflectors with a size of 75 mm  $\times$  55 mm, which can obtain a high reflectivity and a prevention of double image, in comparing with normal glass mirrors. The separating distance between the two adjust mirror is 310 mm, and both can be rotated downward for 20 degrees to keep the object right in the center of visual field. A single picture captured by this system is with a 5184  $\times$  3456 pixel resolution, it is cut out into two stereo pictures of .tif files both with a 2250  $\times$  2600 pixel resolution, as shown in Fig. 5. Because the two pictures are taken from the same time, so the stereo pictures are exactly synchronous.

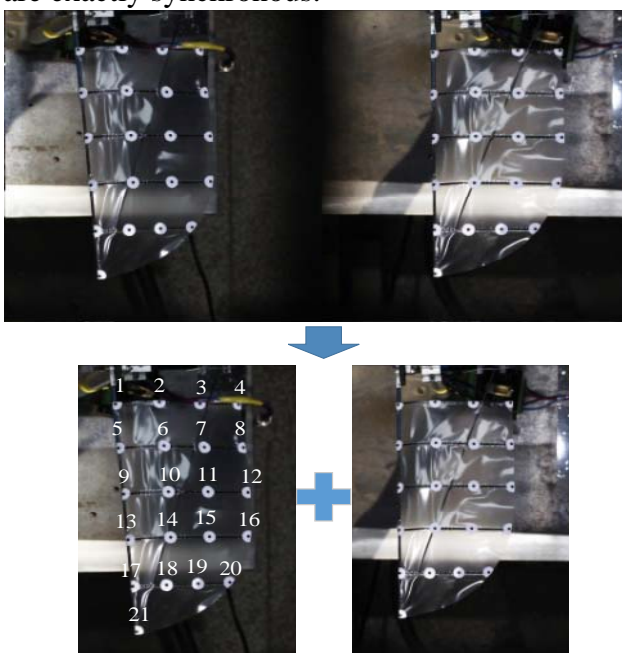


Fig. 5 Stereo pictures taken by the DIC system

External speedlight is used to illuminate the flapping-wing. High-speed synchronous flash mode is used in according with the high shutter speed of the camera. The illumination of the speedlight is more than 20000 lux, it is obvious that any other light sources is not in the same order than speedlight, therefore large depth of field and high speed of shutter are simultaneously satisfied in this case. The setting of the speedlight is automatically modulated by camera's internal photometry, it is very easy to obtain a right exposure rather than tedious adjustments.

The DIC system take pictures through a glass window on the upper surface of the wind tunnel. It is mounted just above the position of the left wing, which is marked with circular dots. These marks are printed on paper and then pasted on the skeleton.

The shutter of the camera is released by a trigger signal which is generated by a data acquisition card (DAQ) of National Instruments USB-6251, this DAQ card is also used for synchronously measuring the aerodynamic forces and flapping kinematics of the flapping-wing.

Because the camera and speedlight comprise a low-speed system (the interval between every two pictures is about 0.1~2.5 s for speedlight charging), the deformation process are recorded by substitute image sequences, whose pictures are triggered at a progressing moment in each repeating cycle. This is similar to what can be taken with a high-speed system, premising that there is no cycle-to-cycle variation.

### 3 Experimental Procedure

The experimental procedure includes four stages, which are parameters setting, operation, data acquisition, and data processing. A virtual instrument (VI) LabVIEW program is created for this experiment. The program consists of three modules: the first one that communicates to the MCBL 3006C controller of the flapping mechanism via a CAN bus, the second one that communicates to the DAQ card to acquire data from signal conditioner of the Nano17 and sensors mounted on the flapping mechanism,

and the third one control the trigger of the camera via the counter of the DAQ card. All modules can work synchronously with each other.

In the first module, the program initializes CAN network and has the motor controller standing by, then controls the motor to rotate at a precise flapping frequency specified by user. In the second module, the VI first specifies the sampling rate and number of samples per measurement to the DAQ card (In this case, the sample rate is 50000 and the number of samples is 50, meaning that time of the measurement is 1/1000 s). Then the DAQ card start data acquisition intermittently with an interval time calculated by the third module. The third module is used to calculate the trigger moments of sampling and picturing. The time interval between each trigger is determined by the following relationship:

$$\Delta T = (N + 1/n) / f \quad (1)$$

where  $\Delta T$  is the trigger time interval,  $n$  is the number of recording per cycle,  $f$  is the flapping frequency, and  $N$  is the number of complete cycles between sequential triggers.

The operation sequence is as follows. The user first defines a flapping frequency  $f$ , record number  $n$ , and cycle period interval  $N$ , after that, the VI program initializes the motor controller and the DAQ card. Then the user calibrates the DIC system by using a calibration board provided by Correlated Solution, Inc. After all facilities are standby, the wind tunnel and the flapping mechanism are activated. Then a button is pressed to start the picturing and sampling sequences, until the record number  $n$  is achieved. In this study, about 30 frames of pictures and measurement data are taken in each run. This procedure outputs the .xls files for measurements and .tif files for DIC measurements. Each .xls files contains about 2 cycles data, with a  $11 \times 30$  array including time sequences, aerodynamic forces (6 components), flapping angle, input current, input voltage and the flapping torque.

## 4 Data Postprocessing

Commercial software VIC3D of Correlated Solution™ is used for correlation analysis. The program correlates each pair of .tif files and outputs the coordinates of data points on the wing surface into .csv files. These coordinates are computed relative to the reference coordinate system of the camera. The displacements can be generated from these coordinates, but are composed of both rigid body motions and structural deformations. It is necessary to separate the two: the latter is much smaller than the former, but is expected to be the dominant factor of aerodynamic forces. Because of using trace points, full-field deformation cannot be obtained. Thus, the software's auto function of 'removing the rigid body displacement' is not available for structural deformation calculation. The rigid body displacement and local structural deformations are separated by creating a virtual undeformed wing at the same flapping angle as the deformed wing measured during flapping. This is done by first organizing a reference plane by three points of 1, 4, 5 (as shown in Fig. 5), it is assumed that the plane follows the wing kinematics, because these three points are close to the wing root and the elastic deformation can be neglected. Then the distance  $d_n$  from the marker points to the reference plane can be computed, where  $n$  is the number of marker points. The deformation of the wing during flapping is expressed as follows:

$$D_n = d_n - d'_n \quad (2)$$

where  $d'_n$  is the distance computed from a static wing. The tip deflection  $i = D_{21}$  (the effect of wing bending, in millimeters) and the angle of twist  $\alpha_{twist} = \arcsin(D_{20} / c_{0.8})$  (measured at 80% of the wing length, where the chord length is  $c_{0.8}$ , defined as positive when the trailing edge is below the leading edge) are two parameters chosen to describe the wing deformation.

The experiment is designed to obtain a relationship between the aerodynamic performance, efficiency and the related structural deformation of flapping wings when it is in forward flight. Data of periodic averaged forces, power consumption, kinematics, and

flexible deformation are collected for analysis. The input power of the wing is calculated as

$$P_{in} = \omega M = \dot{\phi} M \quad (3)$$

where  $\omega$  is the angular velocity which can be derived from the flapping angle and  $M$  is the flapping torque. The power consumption is converted into power-to-weight ratio, evaluating the lift generated for each unit of power input. The efficiency of the flapping wing is calculated as

$$\eta = P_{out} / P_{in} = TV / P_{in} \quad (4)$$

where  $T$  is the thrust,  $V$  is the free stream speed. It is notable that the flapping wing generates thrust and drag simultaneously during flapping flight, it is impossible to measure the thrust (or the drag) independently. For this reason, the thrust is altered by resultant force of thrust and drag for evaluating efficiency (if so, there will be negative efficiency, meaning that the wing absorbs energy from the airflow), which is named as total efficiency.

## 5 Results and Discussions

### 5.1 Wing performance

The flapping wing is evaluated with the aerodynamic performance and the efficiency. The average thrust and lift produced by the wing is shown in Fig. 6. The results show that flapping frequency has a significant effect on thrust production, while the lift is mainly affected by airflow speed. Higher flapping frequency corresponds to stronger inertial and aerodynamic loads imparted on the flapping wings, resulting in larger passive wing deformation. It can be inferred that passive wing deformation is critical to thrust production. As a result, the flexibility design of flapping-wing is the major objective to obtain more thrust in forward flight.

The aerodynamic forces cannot represent the overall performance, because a wing that requires a higher frequency to achieve greater forces may be inefficient [12]. Therefore, the total efficiency and power-to-weight ratio are tested with results illustrated in Fig. 7. It can be seen that the total efficiency is corresponding to

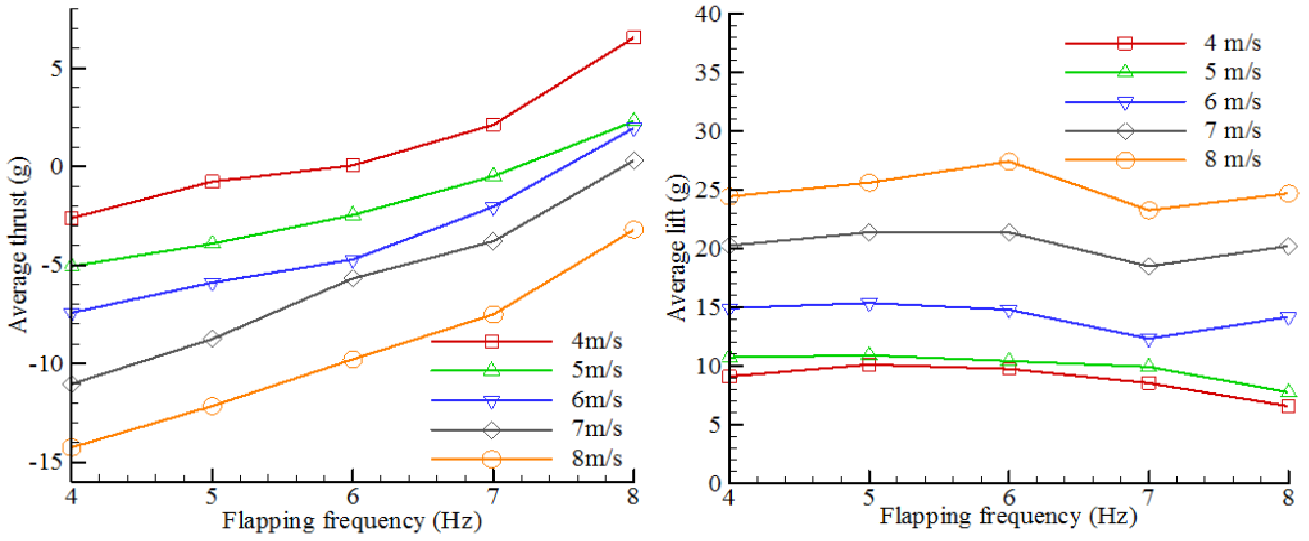
the frequency increment, with a trend that the rising speed slows down and reaches an ultimate value. It can be inferred that there is a limit of thrust and flying speed, excess deformation may occur when the wing flaps too fast, resulting in a loss of aerodynamic forces. In this case, a frequency of 8 to 10 Hz may obtain a highest efficiency. In Fig. 7b, the power-to-weight ratio decreases when frequency increases, for the input power raises while the lift is not significantly changed (Fig. 6b) under a higher frequency. It is notable that the experiments are carried out arbitrarily. The experimental states are not the conditions that a free flight really needs (lift equals to gravity, and thrust equals to drag). Thus, the power-to-weight results may not fully represent the actual performance of the tested flapping-wing. We suppose that there is also a best condition (a balance of flying speed, angle of attack, and flapping frequency) that the flapping-wing obtains a highest power-to-weight ratio.

### 5.2 Structural Deformation

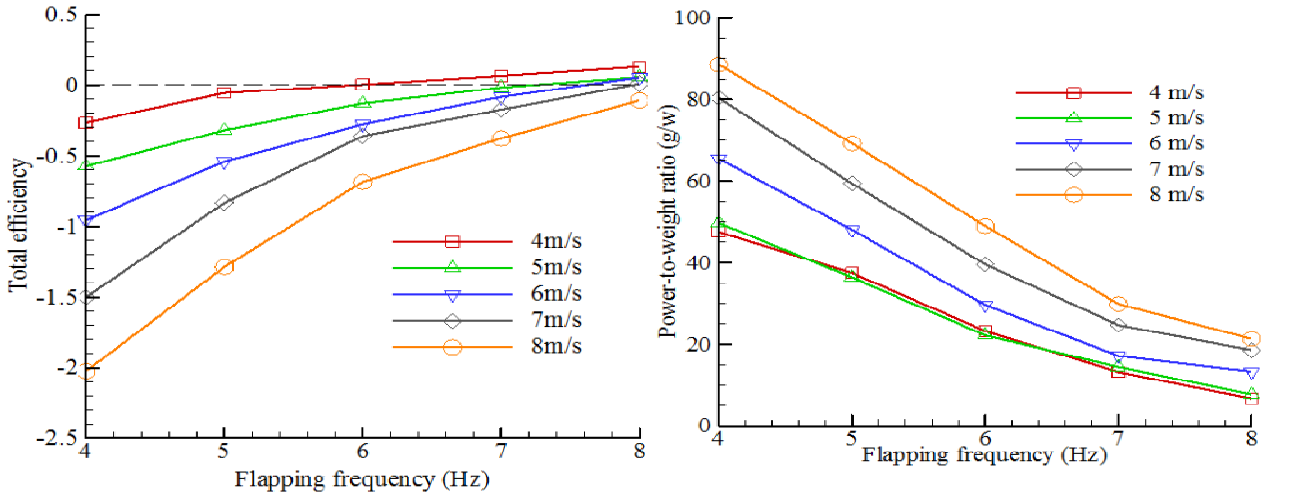
The passive wing deformation is caused by inertial and aerodynamic loads imparted on the flapping wings. Higher frequency will enhance the loads of inertial force and aerodynamic force, thus larger deformation occurs. Fig. 9 depicts the complete cyclic deformation history under flapping frequencies from 4 to 8 Hz and airflow speed from 4 to 8 m/s. It can be seen that the phase loops enclose different areas and are oriented at different phase angles due to differences of frequency and airflow speed. Two scalars of loop enclosed area and phase angle can be used to represent the wing compliance[10]. The phase angle is defined as the angle between the line formed by the maximum and minimum  $y$  values (twist deflection) and the  $x$ -axis, as shown in Fig. 9a. The larger enclosed areas as well as the phase angle, the wing behaviors more flexible.

The result shows that the flapping frequency increases, the loop enclosed area as well as the phase angles increases. However, the wind speed affects little to the passive deformation of the flexible wing, in contrasting with flapping frequency. It can be inferred that,

**EXPERIMENTAL CHARACTERIZATION OF A FLEXIBLE MEMBRANE FLAPPING-WING IN FORWARD FLIGHT**



a) Average thrust of membrane wing      b) Average lift of membrane wing  
**Fig. 6 Aerodynamic performance of the flexible membrane wing**



a) Total efficiency of membrane wing      b) Power-to-weight ratio of membrane wing  
**Fig. 7 Efficiency of the flexible membrane wing**

the passive wing deformation is significantly correlate to the thrust production, by contrasting Fig. 6 and Fig. 9.

Notable phase loop asymmetries can be found in Fig. 9. The enclosed area in downstroke is smaller than upstroke, meaning that during downstroke, the wing deflects smaller than upstroke. This is due to the asymmetries of cambered skeleton and one-sided membrane lamination. Consequently, the effective area for lift is changing during flapping, and cycle average lift is raised by reducing the negative lift produced in upstroke, as shown in Fig. 8.

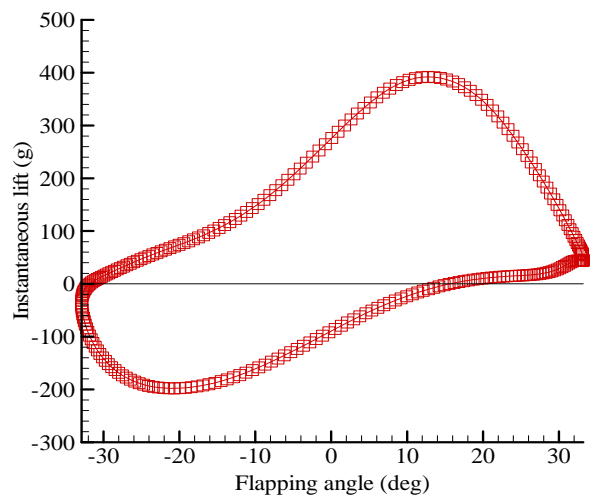


**Fig. 8 Structural deformation at different frequencies and airflow speed**

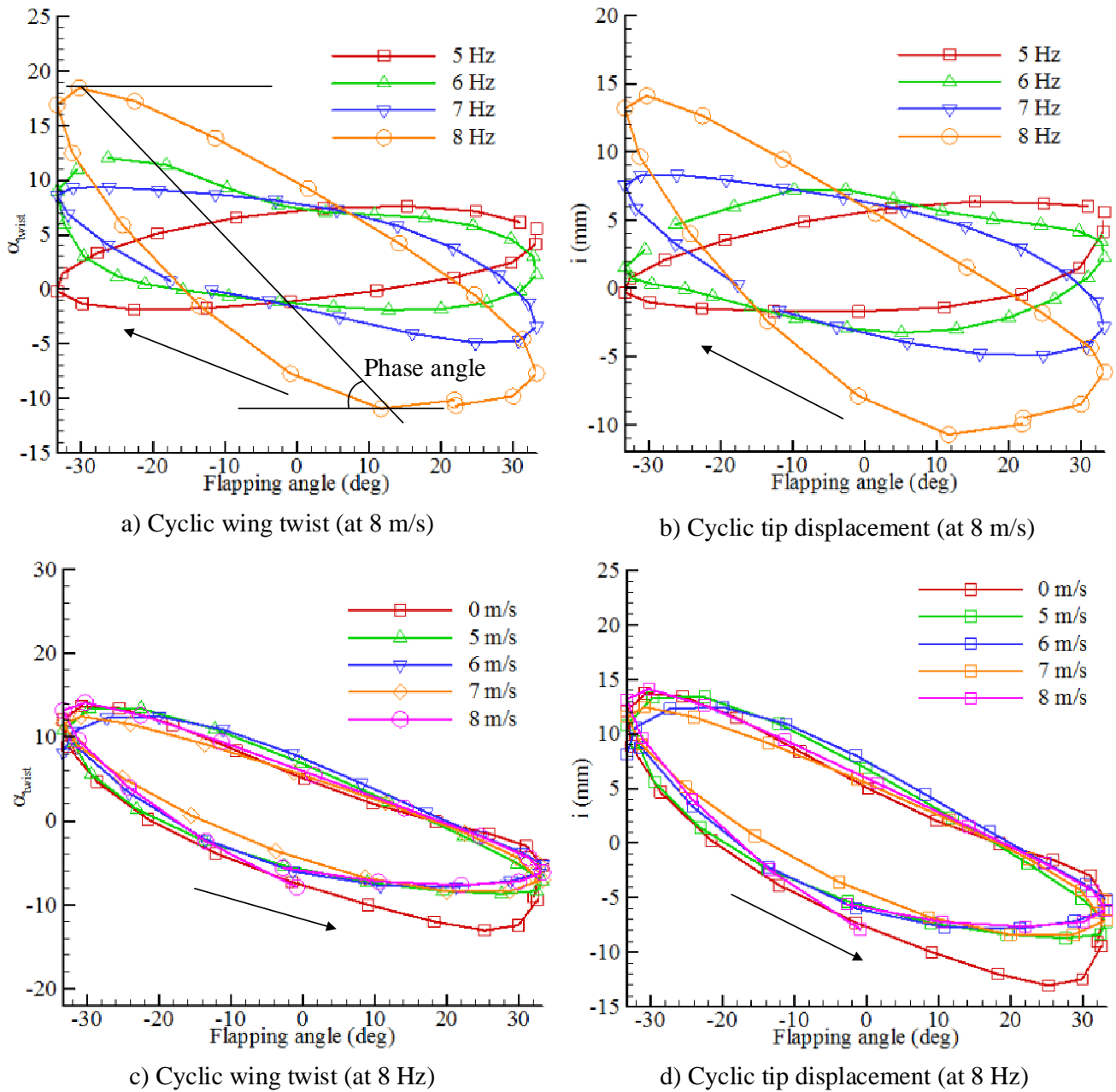


Fig. 9 Structural deformation at different frequencies and airflow speed

## 6 Conclusions

This paper has detailed a multidisciplinary experimental study towards the experimental characterization of flexible membrane flapping-wing. An experimental setup is developed for studying the relationship between wing passive deformation and aerodynamic forces of a micro flexible membrane flapping-wing, which is constructed by carbon fiber skeleton and polyether film membrane. The wing is actuated by a flapping mechanism which is produced for

flapping in an accurate frequency and capable of measuring power consumption and flapping kinematics. A unique DIC system with only one single camera is developed for exactly synchronous capturing stereo pictures, and the corresponding method for obtaining deformation sequences with other multi-parameters is presented.

Different tests have been performed to characterize the wing's structural properties and performance. The wing deformation is measured as well as the average aerodynamic forces and power efficiency under different

wind speed and flapping frequency. As the results of the tests shown, flapping frequency affects the passive deformation significantly, resulting in a strong correlation between the flexibility and the thrust. Another relationship can also be found between the asymmetrical deformation and the average lift, specific deformation pattern is suggested to generate higher average lift.

## References

- [1] Abate, G., and Shyy, W. Introduction: Biologically Inspired Aerodynamics. *AIAA Journal*, Vol. 46, No. 9, pp. 2113–2114, 2008.
- [2] Ellington C.P, Berg C. van den, Willmott, A.P. and Thomas. Leading-edge vortices in insect flight. *Nature*, Vol. 384, Issue 19/26, PP 626–630, 1996.
- [3] Dickinson M.H, Lehmann F.O and Sane S.P. Wing Rotation and the Aerodynamic Basis of Insect Flight. *Science*, Vol. 284, No. 5422, PP 1954 – 1960, 1999.
- [4] Zeng, L., Hao, Q., and Kawachi, K. A Scanning Projected Line Method for Measuring a Beating Bumblebee Wing. *Optics Communications*, Vol. 183, No. 1–4, pp. 37–43, 2000.
- [5] Wang, H., Zeng, L., Liu, H., and Yin, C. Measuring Wing Kinematics, Flight Trajectory and Body Attitude During Forward Flight and Turning Maneuvers in Dragonflies. *Journal of Experimental Biology*, Vol. 206, No. 4, pp. 745–757, 2003.
- [6] Walker, S., Thomas, A., and Taylor, G. Photogrammetric Reconstruction of High-Resolution Surface Topographies and Deformable Wing Kinematics of Tethered Locusts and Free-Flying Hoverflies. *Journal of the Royal Society Interface*, Vol. 6, No 33, pp. 351–366, 2009.
- [7] Walker, S., Thomas, A., and Taylor, G. Deformable Wing Kinematics in the Desert Locust: How and Why do Camber, Twist and Topography Vary Through the Stroke?. *Journal of the Royal Society Interface*, Vol. 6, No. 38, pp. 735–747, 2009.
- [8] Young, J., Walker, S., Bomphrey, R., Taylor, G., and Thomas, A. Details of Insect Wing Design and Deformation Enhance Aerodynamic Function and Flight Efficiency. *Science*, Vol. 325, No. 18, pp. 1549–1552, 2009.
- [9] Wu, P., Stanford, B., Bowman, W., Schwartz, A., and Ifju, P. Digital Image Correlation Techniques for Full-Field Displacement Measurements of Micro Air Vehicle Flapping Wings. *Experimental Techniques*, Vol. 33, No. 6, pp. 53–58, 2009.
- [10] Wu, P., Ifju, P., and Stanford, B. Flapping Wing Structural Deformation and Thrust Correlation Study with Flexible Membrane Wings. *AIAA Journal*, pp. 53–58, 2009.
- [11] Cheng K. H., James E., Sunil V. and Huang P. G.. Development of flapping wing micro air vehicles - design, CFD, experiment and actual flight. *48th AIAA Aerospace Sciences Meeting Including the New Horizons Forum and Aerospace Exposition*, Orlando, Florida. AIAA 2010-1018, 2010.
- [12] Shyy, W., Lian, Y., Tang, J., Viieru, D., and Liu, H.. *Aerodynamics of Low Reynolds Number Flyers*. Reissue, Cambridge University Press, 2011.

Mail to: wlg@nwpu.edu.cn

## Copyright Statement

The authors confirm that they, and/or their company or organization, hold copyright on all of the original material included in this paper. The authors also confirm that they have obtained permission, from the copyright holder of any third party material included in this paper, to publish it as part of their paper. The authors confirm that they give permission, or have obtained permission from the copyright holder of this paper, for the publication and distribution of this paper as part of the ICAS 2014 proceedings or as individual off-prints from the proceedings.